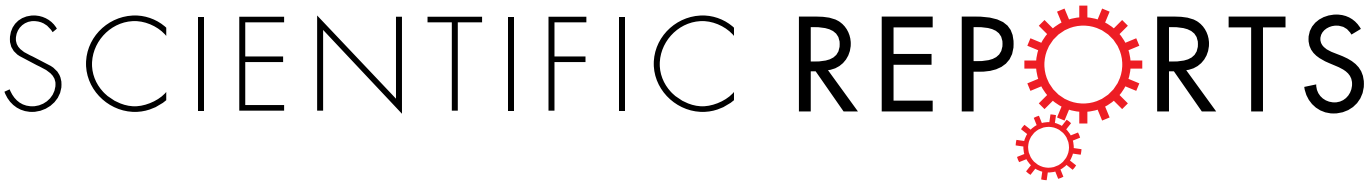

OPEN

Nanostructured $MoS_2/BiVO_4$ Composites for Energy Storage Applications

Received: 12 July 2016
Accepted: 13 October 2016
Published: 03 November 2016

Yukti Arora[1], Amit P. Shah[2], Shateesh Battu[3], Carina B. Maliakkal[2], Santosh Haram[3], Arnab Bhattacharya[2] & Deepa Khushalani[1]

We report the optimized synthesis and electrochemical characterization of a composite of few-layered nanostructured MoS_2 along with an electroactive metal oxide $BiVO_4$. In comparison to pristine $BiVO_4$, and a composite of graphene/$BiVO_4$, the $MoS_2/BiVO_4$ nanocomposite provides impressive values of charge storage with longer discharge times and improved cycling stability. Specific capacitance values of 610 Fg^{-1} (170 $mAhg^{-1}$) at 1 Ag^{-1} and 166 Fg^{-1} (46 $mAhg^{-1}$) at 10 Ag^{-1} were obtained for just 2.5 wt% MoS_2 loaded $BiVO_4$. The results suggest that the explicitly synthesized small lateral-dimensioned MoS_2 particles provide a notable capacitive component that helps augment the specific capacitance. We discuss the optimized synthesis of monoclinic $BiVO_4$, and few-layered nanostructured MoS_2. We report the discharge capacities and cycling performance of the $MoS_2/BiVO_4$ nanocomposite using an aqueous electrolyte. The data obtained shows the $MoS_2/BiVO_4$ nanocomposite to be a promising candidate for supercapacitor energy storage applications.

The ever-increasing global energy demands have spurred increased research into energy harvesting and storage systems[1,2]. The development of effective energy storage systems with high energy density as well as high power density is becoming increasingly important. Electrochemical capacitors, also termed as supercapacitors, have attracted significant interest as these devices bridge the energy density gap between conventional capacitors and batteries. Layered inorganic systems exhibit unusual properties that are technologically important. The unique mechanical, electronic, thermal and optical properties of graphene and other two-dimensional layered materials like the transition metal dichalcogenides (TMDCs) such as molybdenum disulfide (MoS_2) have enabled them to be utilized for various novel applications[3–6]. One specific application for which these layered materials have been recently explored is in energy storage devices, such as lithium-ion batteries and supercapacitors[7,8]. The recent proliferation of research into 2D layered chalcogenides is the result of their intrinsic high ionic conductivity, high surface area, inherent chemical stability (under a variety of pH conditions) and propensity for charge storage[9,10].

In this work, an electroactive metal oxide $BiVO_4$ is combined with few-layered nanostructured (NS) MoS_2 as a capacitive component to form a hybrid structure. It should, however, be noted that over the last few years several studies that quantify the capacitive storage of MoS_2 have been reported[11–22]; these typically use MoS_2 in conjunction with a variety of carbon allotropes, predominantly graphene (r-GO). Interestingly, as yet MoS_2 has not been coupled with a viable electrochemical component to form a hybrid supercapacitor. Table 1 shows a summary of a few different approaches; the specific capacitance values vary between 100 and 550 Fg^{-1} with an average of *ca.* 250 Fg^{-1}. Moreover this value is highly dependent on type of MoS_2 (bulk *vs.* nanostructured), manner of synthesis of nanostructured MoS_2 (exfoliated *vs.* synthesized from precursors), current density employed and the amount of loading of MoS_2 to the carbon source.

Another approach to augment the specific capacitance of electric double-layer capacitors is to incorporate a new electroactive material along with a potent capacitive component to enable high energy density supercapacitors while maintaining high power operations. It has been reported that MoS_2 suffers from low conductivity, low theoretical specific capacity and easy restacking of the sheets[23,24]. Despite the aforementioned limitations of MoS_2,

[1]Department of Chemical Sciences, Tata Institute of Fundamental Research, Mumbai-400005, India. [2]Department of Condensed Matter Physics and Materials Science, Tata Institute of Fundamental Research, Mumbai-400005, India. [3]Department of Chemistry, Savitribai Phule Pune University, Ganeshkhind, Pune-411007, India. Correspondence and requests for materials should be addressed to S.H. (email: haram@chem.unipune.ac.in) or A.B. (email: arnab@tifr.res.in) or D.K. (email: khushalani@tifr.res.in)

Type of MoS_2	Type of carbon nanostructure	Loading %	Electrolyte	Current density/ Scan rate	Specific capacitance
Bulk MoS_2[11]	Porous carbon tubes	Not provided	3.0 M KOH	$1\,Ag^{-1}$	**$210\,Fg^{-1}$**
Few layered MoS_2[12]	Graphene	Not provided	1 M $HClO_4$	$1\,Ag^{-1}$	**$243\,Fg^{-1}$**
Few layered MoS_2[13]	Graphene (r-GO)	17.6 wt% MoS_2 loaded on r-GO	1 M $HClO_4$	$10\,mVs^{-1}$	**$265\,Fg^{-1}$**
Few layered MoS_2[14]	Graphene	Not provided	1 M $HClO_4$	$20\,mVs^{-1}$	**$282\,Fg^{-1}$**
MoS_2 (bulk)[15]	Graphene (r-GO)	50% r-GO loading	1 M H_2SO_4	$5\,mVs^{-1}$	**$416\,Fg^{-1}$**
3-D tubular MoS_2[16]	Polyaniline	PANI is 60% loaded	1 M H_2SO_4	$0.5\,Ag^{-1}$	**$552\,Fg^{-1}$**
MoS_2 nanosheets (bulk)[17]	—	—	1 M Na_2SO_4	$0.5\,Ag^{-1}$	**$92\,Fg^{-1}$**
MoS_2 nanospheres (bulk)[18]	—	—	1 M KCl	$1\,Ag^{-1}$	**$122\,Fg^{-1}$**
MoS_2 nanosheets[19]	—	—	1 M Na_2SO_4	$1\,Ag^{-1}$	**$129.2\,Fg^{-1}$**
Monolayer MoS_2[20]	—	—	0.5 M H_2SO_4	$20\,mVs^{-1}$	**$\sim 140\,Fg^{-1}$**
MoS_2 nanoflowers[21]	—	—	1 M KCl	$1\,Ag^{-1}$	**$168\,Fg^{-1}$**
Mesoporous MoS_2[22]	—	—	1 M KCl	$1\,mVs^{-1}$	**$403\,Fg^{-1}$**
Few layered nanostructured $MoS_2/BiVO_4$ – This work	—	***2.5 wt% MoS_2 loaded on $BiVO_4$***	***2 M NaOH***	***$1\,Ag^{-1}$***	***$610\,Fg^{-1}$***

Table 1. Comparison of supercapacitor performance of MoS_2/carbon nanostructures and bare MoS_2.

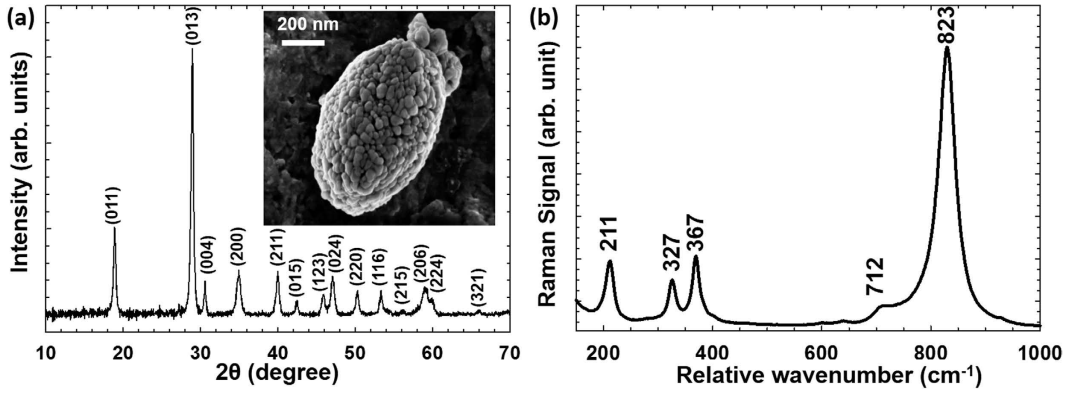

Figure 1. (**a**) XRD pattern of $BiVO_4$, in the inset: SEM image of solvothermally synthesized $BiVO_4$ and (**b**) Raman spectrum indicating various vibrational modes of $BiVO_4$.

it is being employed in electrochemical devices *albeit* in conjunction only with carbon nanostructures so as to overcome these limitations.

As mentioned above, here we report a $BiVO_4/MoS_2$ composite, with the first ever usage of bare MoS_2 as the capacitive component. The MoS_2 has been synthesized from thermolysis of $(NH_4)_2MoS_4$ in the presence of H_2. The resulting $MoS_2/BiVO_4$ nanocomposite has demonstrated much larger values of charge storage, longer discharge times and improved cycling stability in comparison to pure $BiVO_4$ itself, or graphene/$BiVO_4$ composites. NS $MoS_2/BiVO_4$ composites have been found to be superior to graphene/$BiVO_4$ composites, and hence a promising candidate for supercapacitor applications.

Results and Discussion

In this study, three types of samples were investigated: pure $BiVO_4$, a composite of 2.5 wt% graphene/$BiVO_4$ and a composite of 2.5 wt% NS $MoS_2/BiVO_4$. These are labeled as $BiVO_4$, $BiVO_4$-G and $BiVO_4$-M for succinctness in the following sections. Details of the synthesis of all these samples are discussed in the methods section.

$BiVO_4$ was synthesized by a solvothermal route. The purity and crystallinity of solvothermally synthesized $BiVO_4$ was analyzed by high-resolution X-ray diffraction (XRD), Fig. 1a. The peaks in the diffractogram could be indexed according to JCPDS card no. 75–2480, corresponding to a monoclinic scheelite structure. The inset in Fig. 1a shows an SEM image of $BiVO_4$. It can be seen that 10–20 nm diameter spherical $BiVO_4$ particles agglomerate to form larger porous oval shaped clusters with average size in the range 200–300 nm. Figure 1b shows a Raman spectrum of $BiVO_4$. The most intense Raman band at around 823 cm^{-1} is assigned to the V-O symmetric stretching mode, while the weak shoulder at around 712 cm^{-1} is due to V-O antisymmetric stretch. The band at 211 cm^{-1} is related to external mode (translation/rotation) of $BiVO_4$, and the bands at 367 and 327 cm^{-1} are ascribed to the symmetric and asymmetric deformation modes of the VO_4^{3-} tetrahedron, respectively[25].

Figure 2a shows the XRD profile of the nanostructured MoS_2 grown on sapphire via a two-step thermolysis process. The diffraction pattern from the sample ((002) peak) is indexed to MoS_2, indicating periodicity along the *c*-axis. All other peaks in the XRD correspond to *c*-sapphire (substrate). The samples, after the first annealing step,

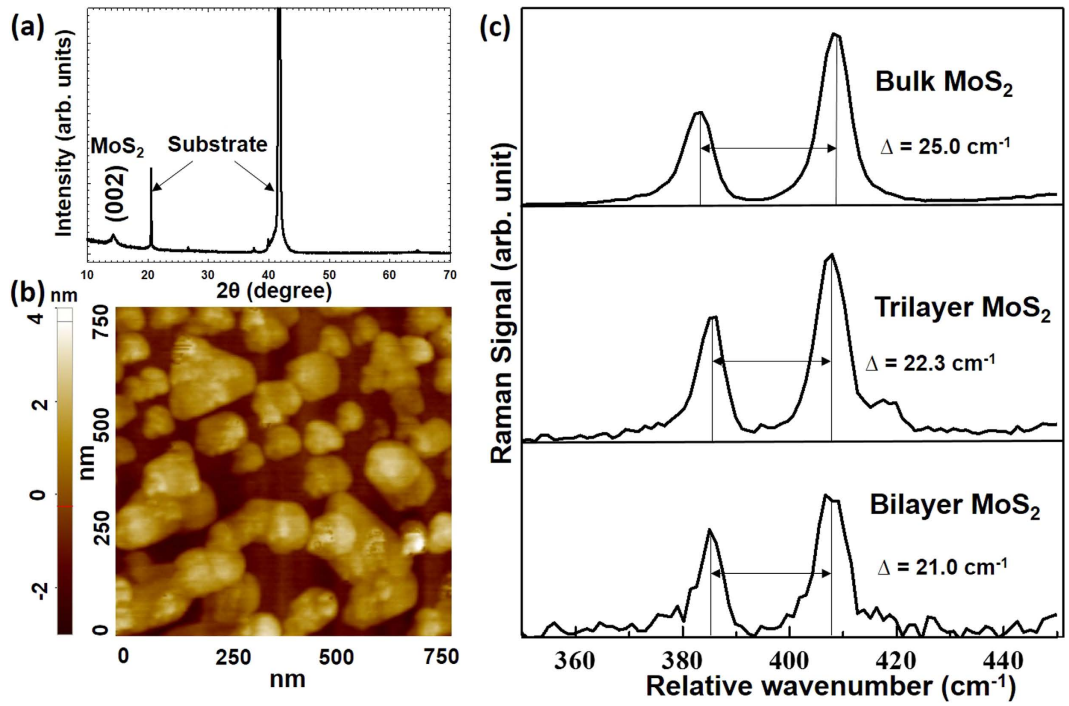

Figure 2. (**a**) XRD showing (002) peak of MoS_2, (**b**) AFM topographic image of nanostructured MoS_2 grown on sapphire, and (**c**) Raman spectra of bilayer, trilayer and bulk MoS_2.

were subjected to a second annealing at 1000 °C in the mixture of N_2 and sulfur. The addition of sulfur before the second annealing process greatly improved the crystallinity[26].

An atomic force microscopy (AFM) image of the MoS_2/sapphire sample obtained after second annealing in the presence of sulfur is shown in Fig. 2b. From the height of the flakes we can infer the presence of monolayer, bilayer and trilayer regions along with bulk MoS_2, Fig. S1. The lateral dimension of the flakes are about 50–200 nm.

Figure 2c shows the Raman spectra for MoS_2 flakes of different thickness on sapphire substrates, obtained using laser excitation at 532 nm. The energy difference (Δ) between two Raman peaks (modes A_{1g} and E_{2g}) can be used to identify the number of MoS_2 layers on the substrate[26]. The values of Δ obtained for different parts of the sample are in the range 21–23 cm^{-1} and 25 cm^{-1}, which suggests the presence of nanostructured MoS_2 (mono/bi/tri-layer) and bulk respectively[26]. It should be noted that normally the spatial resolution of the Raman spectra, being limited by the laser spot size, is poorer than that of an AFM. So the Raman signal is actually averaged over different MoS_2 flakes even when it is acquired from a single 'spot'. We have therefore observed that it is difficult to differentiate a monolayer flake from a bilayer flake if the lateral sizes of the flakes are too small using only Raman spectroscopy. As such, further characterization was done by Raman imaging of a larger area (8μm x 8μm) of MoS_2 on sapphire sample (Supporting Information Fig. S2). The image was acquired using a range of minimum value of 383.6 cm^{-1} (belonging to ideally bulk MoS_2) to a maximum value of 384.8 cm^{-1} (ideally belonging to few layers of MoS_2). As such, most of the image depicts that the sample shows a Raman signal closer to that of few layers of MoS_2. From combined information provided by Raman mapping and AFM, it can therefore be concluded that the MoS_2 film on the substrate consists of mostly nanostructured MoS_2 and a few thicker flakes (≥5 monolayers).

To effectively recover nanostructured MoS_2 from sapphire, the sample was simply peeled off using a surgical blade. Following this recovery, the MoS_2/$BiVO_4$ composite was prepared via ultrasonication. 2.5wt% NS MoS_2 was loaded on $BiVO_4$. Analogously, a graphene/$BiVO_4$ composite was also prepared by ultrasonicating commercially-procured graphene with $BiVO_4$. The two components in the composite (the 2D layered material and $BiVO_4$) are expected to interact via van der Waals' interactions. Figure 3a, shows XRD profiles of $BiVO_4$-G and $BiVO_4$-M, all the peaks can be indexed to $BiVO_4$. XRD patterns show well resolved peaks of monoclinic $BiVO_4$, and there were no deleterious effects observed due to ultrasonication. The peaks due to diffraction from the MoS_2 lattice planes were however not observed in the diffractogram, perhaps due to the very small amount of MoS_2 present and lack of a preferential orientation following delamination from the original sapphire substrate. Figure 3b shows Raman spectrum of $BiVO_4$-G obtained using laser excitation at 532 nm. All vibrational modes of $BiVO_4$ are observed along with vibrational signatures of graphene (D- and G- bands). Figure 3c and d show SEM images of $BiVO_4$-G and $BiVO_4$-M composites respectively. These images clearly show the two separate phases of capacitive components and $BiVO_4$. The energy-dispersive X-ray pattern for $BiVO_4$-M confirmed the presence of Bi, V and Mo (Fig. S3).

Electrochemical characterization. The electrochemical behavior of all three samples ($BiVO_4$, $BiVO_4$-M and $BiVO_4$-G) was evaluated by performing cyclic voltammetry, charge discharge and cycling stability, using the same working electrode.

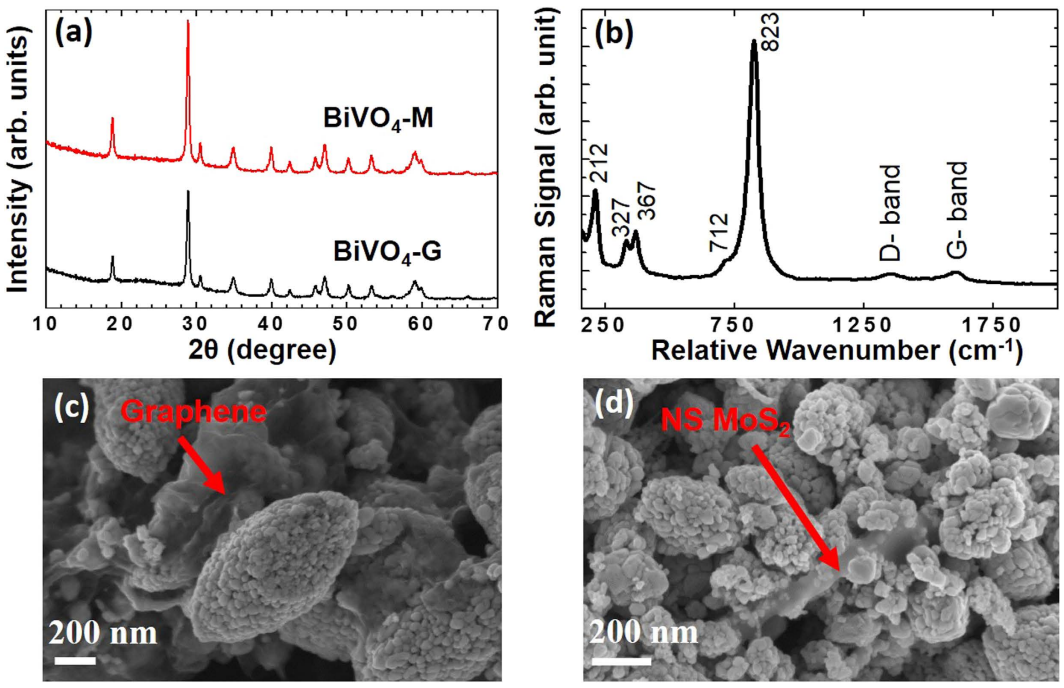

Figure 3. (**a**) XRD profiles of $BiVO_4$-G and $BiVO_4$-M, all peaks can be indexed to $BiVO_4$ which indicates chemical integrity of $BiVO_4$ is intact, (**b**) Raman spectrum of $BiVO_4$-G showing vibrational features of both $BiVO_4$ and graphene, (**c**,**d**) show SEM images of $BiVO_4$-G and $BiVO_4$-M.

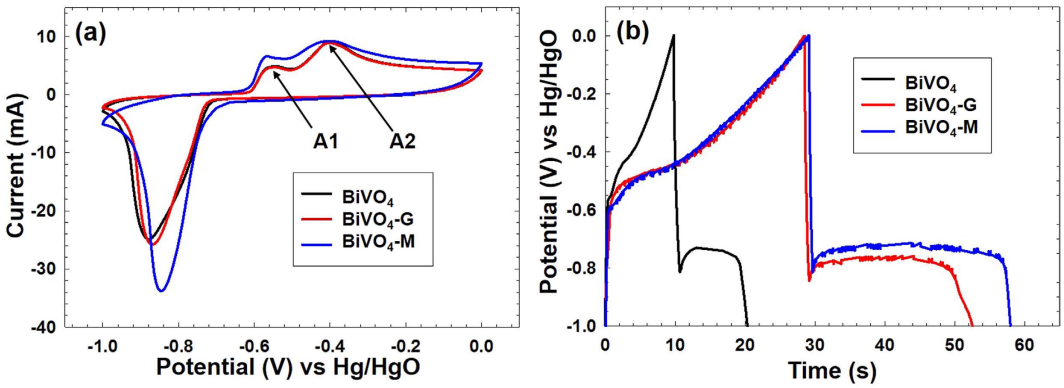

Figure 4. (**a**) CV curves of $BiVO_4$, $BiVO_4$-G and $BiVO_4$-M at a scan rate of 20 mVs^{-1}, (**b**) CD profile of $BiVO_4$, $BiVO_4$-G and $BiVO_4$-M at a current density of 7 Ag^{-1}.

Cyclic voltammetry measurements were performed at various scan rates from 5 to 50 mVs^{-1}, the data presented in Fig. 4a is for 20 mVs^{-1} scans (the other scans are shown in the supporting information). Redox peaks in the CV curve can be attributed to quasi-reversible faradaic process ($Bi^{3+} \leftrightarrow Bi^0$). For bare $BiVO_4$, a single peak with high current was assigned to reduction of Bi^{3+} to Bi^0 (−0.85 V), on the other side, two anodic peaks were obtained at -0.52 V and -0.4 V for the oxidation[27,28]. The oxidation peak A1 is assigned to the oxidation of Bi^0 to Bi^+ and peak A2 is assigned to the oxidation of Bi^+ to Bi^{3+}. Further, the CV profiles for $BiVO_4$-G and $BiVO_4$-M in Fig. 4a matched well with CV curve of pristine $BiVO_4$ indicating redox peaks were due to $BiVO_4$ and the presence of MoS_2 or graphene did not affect its electrochemical response. No extra peaks are visible for $BiVO_4$-M suggesting that the small fraction of MoS_2 did not show any charge transfer activity in the applied potential window that was operative. With increasing scan rates the oxidation peak potentials shift towards positive direction and reduction peak potentials shift towards negative direction, which is mainly attributed to IR drop component, which dominates at higher current values. The kinetics of interfacial faradaic redox reaction was rapid enough, as an increase in current response at higher scan rates was observed, (see Fig. S4a in the supporting information)[28].

The electrochemical capacitance of $BiVO_4$, $BiVO_4$-M and $BiVO_4$-G was evaluated by galvanostatic charge discharge (CD) measurements. For all the samples, 5 cycles for all current densities were carried out; Fig. 4b presents the data of the 2nd cycle in each case. CD profile of $BiVO_4$ indicated pseudo-capacitive nature of material for charge storage applications. Similar to $BiVO_4$, CD curves of $BiVO_4$-M and $BiVO_4$-G (Fig. 4b) between potential

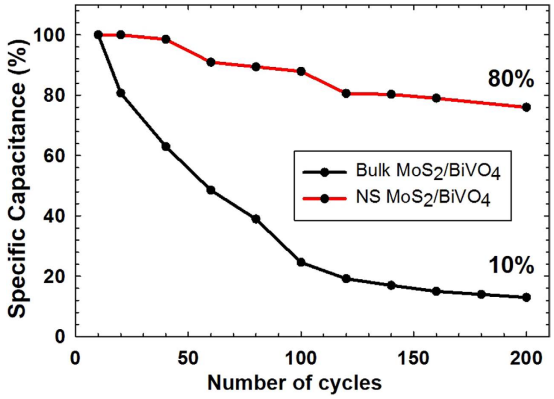

Figure 5. Cycling performance in terms of specific capacitance (%) of Bulk $MoS_2/BiVO_4$ and $BiVO_4$-M at a current density 3 Ag^{-1}.

window −1.0 V to 0.0 V appeared to be non-symmetric, insinuating battery behavior and showing the IR drop. Despite the steep voltage drop, prolonged plateau of voltage output was observed, which is due to the involvement of faradaic process in $BiVO_4$. Using equation, $C = \frac{I\Delta t}{m\Delta V}$ specific capacitance values were obtained. Specific capacitance of $BiVO_4$-M was found to be (212 Fg^{-1} at 3 Ag^{-1}) which is not only higher than bare $BiVO_4$ (108 Fg^{-1} at 3 Ag^{-1}) but at higher current densities it is surpassing specific capacitance obtained for $BiVO_4$-G (Table S1). Figure 4b shows CD profiles of pristine $BiVO_4$, $BiVO_4$-M, and $BiVO_4$-G at a current density 7 Ag^{-1}, which clearly indicates nanostructured MoS_2 composite with $BiVO_4$ has maximum specific capacitance. Generally, the boost of current density results in fading of specific capacitance which is primarily due to inaccessibility of inner electroactive sites to the electrolyte ions due to diffusion limitations (Fig. S4b)[29]. However, even at higher current densities the specific capacitance values are found to be 166.6 Fg^{-1} and 156 Fg^{-1} at 10 Ag^{-1} and 15 Ag^{-1}, respectively, which are impressive. High capacitance values at faster charging rates can be explained by the fact that transition metal dichalcogenides show higher ionic diffusivity as a consequence of large anionic polarizability[30]. For comparison, 2.5 wt% bulk MoS_2 loaded $BiVO_4$ was also prepared via ultrasonication and electrochemical behavior of the same was studied. Although the capacitance values of bulk $MoS_2/BiVO_4$ were higher than nanostructured $MoS_2/BiVO_4$, the composite with the bulk appears to show poor cycling stability (Fig. 5). It was observed that discharge capacity was retained only 10% up to 200 cycles for $BiVO_4$-Bulk MoS_2 composite. On the other hand, $BiVO_4$-M exhibited better long term stability, as it could retain ~80% of the initial value after 200 cycles, for the same current density used for charging (3 Ag^{-1}). The excellent structural and mechanical stability shown by $BiVO_4$-M composite can be ascribed to the high elasticity of nanostructured MoS_2. As depicted by the AFM topographic image, the synthesis method reported here yielded MoS_2 with a lateral particle size of a few 100 nm. It has been purported that as the lateral size of MoS_2 is decreased, there is a higher preponderance of step-edges, and low-coordination edge and corner atoms as compared to basal plane atoms[31]. The effect of these states dominate over those of the basal atoms and can contribute to higher charge storage sites. In addition, since the particles are made up of a few-layered sheets, it has been highlighted by Chhowalla *et al.*[9] that such loosely stacked sheets are able to accommodate structural changes in a better manner upon cycling when compared to bulk MoS_2. The latter has shown large structural instability especially as anodes in lithium ion batteries. As such, when evaluated in unison, the explicitly synthesized small lateral-dimensioned particles which consist of only a few layers of MoS_2 appear to contribute substantially to the charge storage, discharge times and cycling stability of the $MoS_2/BiVO_4$ composite synthesized in this report.

Methods

Analytical reagent grade ammonium metavanadate (NH_4VO_3), sodium dodecyl sulfate (SDS) and anhydrous glycerol were purchased from Merck, India. Polyvinlydene fluoride (PVDF), N-methyl-2-pyrrolidinone (NMP) and activated carbon (AC) were purchased from Himedia, India whereas bismuth nitrate pentahydrate ($Bi(NO_3)_3.5H_2O$) was purchased from Sigma Aldrich. Research grade graphene dispersion in water was procured from US Research Nanomaterials Inc. All chemicals were used as received without further purification.

Synthesis of monoclinic-$BiVO_4$. $BiVO_4$ was prepared by following earlier work reported by Khan *et al.*[28] Typically, 3 mmol of SDS was dissolved in 40 mL of solvent (DI water and glycerol with volume ratio 1:1) in a flask at room temperature. 1 mmol $Bi(NO_3)_3.5H_2O$ and 1 mmol NH_4VO_3 was added to the above clear solution under constant stirring in sequence. After stirring for 7 minutes, the solution was transferred into a stainless steel autoclave with a Teflon liner and heated at 160 °C for 18 hours. After cooling to room temperature, the reaction mixture was centrifuged and the pellet was washed with water and ethanol. Finally, the product was dried under vacuum at 70 °C for *ca.* 5 hours.

Synthesis of nanostructured MoS_2. Synthesis of few layered MoS_2 was successfully achieved by following a published procedure with major modifications[26]. 25 mg of $(NH_4)_2MoS_4$ was dissolved in 20 mL DMF and sonicated for 20 minutes. 10 μL of this precursor solution was spin coated on sapphire at 3000 rpm for 60 seconds.

The substrate was then heated on a hot plate at 120 °C for 30 minutes. The annealing process was performed in a homemade rapid thermal annealing furnace. The freshly prepared thin $(NH_4)_2MoS_4$ layer was placed on the graphite sample holder in the tube furnace flowing with a gas mixture N_2/H_2. It was then heated at 500 °C and was maintained for 60 minutes under constant flow of N_2/H_2 to efficiently remove residual solvent, ammonia molecules, and other byproducts from the precursor. After this step, the furnace was cooled down to room temperature, following which additional sulfur was introduced to the sample holder and the gas environment was changed to N_2 and after 20 minutes purging to remove any air introduced, the temperature was raised to 1000 °C and was maintained for 30 minutes.

Synthesis of 2.5 wt% nanostructured MoS_2/$BiVO_4$ composite. 0.2 mg of nanostructured MoS_2 was recovered via scraping with a surgical blade and was dispersed in 15 mL water. To this 8 mg $BiVO_4$ was added, and the dispersion was sonicated for 8 hours. The composite was recovered after centrifugation and dried under vacuum at 70 °C for 5 hours.

Synthesis of 2.5 wt% graphene/$BiVO_4$ composite. 1 mg of graphene and 40 mg of $BiVO_4$ were dispersed in 30 mL ethanol, and the dispersion sonicated for 8 hours. The composite was recovered by evaporating the solvent on a hot plate at 90 °C.

Characterization. Powder X-ray diffraction (XRD) measurements from 10° to 70° 2θ were recorded using a PANalytical X'pertpro diffractometer with monochromatic Cu Kα source (λ = 1.54056 Å) operating at 40 kV and 30 mA. The elemental composition and surface morphologies of the samples were investigated by Field Emission Scanning Electron Microscopy (FE-SEM) on a Zeiss Ultra FEG 55 instrument at 5 kV operating voltage. Cyclic voltammetry and galvanostatic charge-discharge (CD) studies of the composites were carried out using Bio-Logic VMP3 Galvanostat/Potentiostat Instruments at room temperature.

Electrode material and electrochemical tests. Electrochemical measurements were carried out in a 2 M aqueous NaOH in a three electrode cell at room temperature. Hg/HgO/$Ca(OH)_2$ and platinum plate were used as reference and counter electrodes, respectively. The active electrode was prepared by mixing electroactive material (80 wt%), activated carbon (15 wt%) and polyvinylidene fluoride (5 wt%) with 1 mL of NMP to form a slurry which was coated and dried on a small piece of graphite plate (area of coating, 1 cm^2).

References

1. Hoel, M. & Kverndokk, S. Depletion of fossil fuels and the impacts of global warming. *Resource and Energy Economics* **18,** 115–136 (1996).
2. Chu, S. & Majumdar, A. Opportunities and challenges for a sustainable energy future. *Nature* **488,** 294–303 (2012).
3. Kim, K. S. *et al.* Large-scale pattern growth of graphene films for stretchable transparent electrodes. *Nature* **457,** 706–710 (2009).
4. Tan, C. & Zhang, H. Two-dimensional transition metal dichalcogenide nanosheet-based composites. *Chem Soc Rev* **44,** 2713–2731 (2015).
5. Voiry, D. *et al.* Conducting MoS_2 nanosheets as catalysts for hydrogen evolution reaction. *Nano Lett* **13,** 6222–6227 (2013).
6. Rao, C. N., Gopalakrishnan, K. & Maitra, U. Comparative Study of Potential Applications of Graphene, MoS_2, and Other Two-Dimensional Materials in Energy Devices, Sensors, and Related Areas. *ACS Appl Mater Interfaces* **7,** 7809–7832 (2015).
7. Wang, G., Zhang, L. & Zhang, J. A review of electrode materials for electrochemical supercapacitors. *Chem Soc Rev* **41,** 797–828 (2012).
8. Wang, X. *et al.* High supercapacitor and adsorption behaviors of flower-like MoS_2 nanostructures. *J. Mater. Chem. A* **2,** 15958–15963 (2014).
9. Chhowalla, M. *et al.* The chemistry of two-dimensional layered transition metal dichalcogenide nanosheets. *Nat Chem* **5,** 263–275 (2013).
10. Lei, B., Li, G. R. & Gao, X. P. Morphology dependence of molybdenum disulfide transparent counter electrode in dye-sensitized solar cells. *Journal of Materials Chemistry A* **2,** 3919–3925 (2014).
11. Hu, B. *et al.* Synthesis of porous tubular C/MoS_2 nanocomposites and their application as a novel electrode material for supercapacitors with excellent cycling stability. *Electrochimica Acta* **100,** 24–28 (2013).
12. Huang, K.-J. *et al.* Layered MoS_2–graphene composites for supercapacitor applications with enhanced capacitive performance. *International Journal of Hydrogen Energy* **38,** 14027–14034 (2013).
13. da Silveira Firmiano, E. G. *et al.* Supercapacitor Electrodes Obtained by Directly Bonding 2D MoS_2 on Reduced Graphene Oxide. *Advanced Energy Materials* **4,** 1301380 (2014).
14. Patil, S., Harle, A., Sathaye, S. & Patil, K. Development of a novel method to grow mono-/few-layered MoS_2 films and MoS_2-graphene hybrid films for supercapacitor applications. *CrystEngComm* **16,** 10845–10855 (2014).
15. Gopalakrishnan, K. *et al.* Performance of MoS_2-reduced graphene oxide nanocomposites in supercapacitors and in oxygen reduction reaction. *Nanomaterials and Energy* **4,** 9–17 (2015).
16. Ren, L. *et al.* Three-Dimensional Tubular MoS_2 /PANI Hybrid Electrode for High Rate Performance Supercapacitor. *ACS Applied Materials & Interfaces* **7,** 28294–28302 (2015).
17. Krishnamoorthy, K., Veerasubramani, G. K., Radhakrishnan, S. & Kim, S. J. Supercapacitive properties of hydrothermally synthesized sphere like MoS_2 nanostructures. *Materials Research Bulletin* **50,** 499–502 (2014).
18. Zhou, X., Xu, B., Lin, Z., Shu, D. & Ma, L. Hydrothermal synthesis of flower-like MoS_2 nanospheres for electrochemical supercapacitors. *Journal of nanoscience and nanotechnology* **14,** 7250–7254 (2014).
19. Huang, K.-J., Zhang, J.-Z., Shi, G.-W. & Liu, Y.-M. Hydrothermal synthesis of molybdenum disulfide nanosheets as supercapacitors electrode material. *Electrochimica Acta* **132,** 397–403 (2014).
20. Acerce, M., Voiry, D. & Chhowalla, M. Metallic 1T phase MoS_2 nanosheets as supercapacitor electrode materials. *Nat Nano* **10,** 313–318 (2015).
21. Wang, X. *et al.* High supercapacitor and adsorption behaviors of flower-like MoS_2 nanostructures. *Journal of Materials Chemistry A* **2,** 15958–15963 (2014).
22. Ramadoss, A., Kim, T., Kim, G.-S. & Kim, S. J. Enhanced activity of a hydrothermally synthesized mesoporous MoS_2 nanostructure for high performance supercapacitor applications. *New Journal of Chemistry* **38,** 2379–2385 (2014).
23. Bissett, M. A., Worrall, S. D., Kinloch, I. A. & Dryfe, R. A. W. Comparison of Two-Dimensional Transition Metal Dichalcogenides for Electrochemical Supercapacitors. *Electrochimica Acta* **201,** 30–37 (2016).

24. Tan, C. & Zhang, H. Two-dimensional transition metal dichalcogenide nanosheet-based composites. *Chemical Society Reviews* **44,** 2713–2731 (2015).
25. Yu, J. & Kudo, A. Effects of Structural Variation on the Photocatalytic Performance of Hydrothermsally Synthesized $BiVO_4$. *Advanced Functional Materials* **16,** 2163–2169 (2006).
26. Liu, K. K. *et al.* Growth of large-area and highly crystalline MoS_2 thin layers on insulating substrates. *Nano Lett* **12,** 1538–1544 (2012).
27. Vivier, V. *et al.* Cyclic voltammetry study of bismuth oxide Bi_2O_3 powder by means of a cavity microelectrode coupled with Raman microspectrometry. *Electrochimica Acta* **46,** 907–914 (2001).
28. Khan, Z., Bhattu, S., Haram, S. & Khushalani, D. SWCNT/BiVO4 composites as anode materials for supercapacitor application. *RSC Advances* **4,** 17378–17381 (2014).
29. Sarma, B., Jurovitzki, A. L., Smith, Y. R., Mohanty, S. K. & Misra, M. Redox-Induced Enhancement in Interfacial Capacitance of the Titania Nanotube/Bismuth Oxide Composite Electrode. *ACS Applied Materials & Interfaces* **5,** 1688–1697 (2013).
30. Zheng, N., Bu, X. & Feng, P. Synthetic design of crystalline inorganic chalcogenides exhibiting fast-ion conductivity. *Nature* **426,** 428–432, (2003).
31. Lauritsen, J. V. *et al.* Size-dependent structure of MoS_2 nanocrystals. *Nat Nano* **2,** 53–58 (2007).

Acknowledgements

Authors are thankful to TIFR's SEM facility (Bhagyashree Chalke, Rudheer Bapat) and XRD facility (Nilesh Kulkarni). Venkata Jayasurya is also thanked for assistance with AFM. The work at TIFR was supported through internal grants 120147 and 12P0168.

Author Contributions

Y.A. performed all the experiments, Y.A. and A.P.S. performed MoS_2 synthesis, Y.A. and S.B. collaborated on the electrochemical measurements, Y.A. and C.B.M. performed Raman measurements, S.H., A.B. and D.K. conceived the experiments and analyzed the results. All contributed to the writing of the manuscript.

Additional Information

Supplementary information accompanies this paper at http://www.nature.com/srep

Competing financial interests: The authors declare no competing financial interests.

How to cite this article: Arora, Y. *et al.* Nanostructured MoS_2/$BiVO_4$ Composites for Energy Storage Applications. *Sci. Rep.* **6**, 36294; doi: 10.1038/srep36294 (2016).

Publisher's note: Springer Nature remains neutral with regard to jurisdictional claims in published maps and institutional affiliations.